Stabilization, Reformation and Melting of Poly(L-Lactide) Crystallites

Tai-Yon Cho, Barbara Heck and Gert Strobl

Physikalisches Institut

Albert-Ludwigs-Universität Freiburg

79104 Freiburg

Germany

Abstract

The large size of the crystallites in poly(L-lactide) and the low growth rate enable detailed time- and temperature-dependent X-ray scattering studies of the ordering processes to be carried out. A layer located intermediate between crystals and melt-like regions is observed which finally takes on crystalline order. Recrystallization processes during heating change the complete stack structure rather than the crystallites individually and produce voids in the stacks. Establishment of a new stable structure after a temperature jump in the melting range can be followed in time. DSC experiments indicate times of melting of the order of minutes.

1 Introduction

Poly(L-lactide) (PLLA) is a semi-crystalline polymer [1] of high crystallinity, with values up to 80%. To achieve such high values samples have to be kept for a sufficiently long time - typically several hours - at temperatures above 130°C. On the other hand, a cooling from the melt with standard rates leaves PLLA amorphous or produces - at temperatures between 120°C and the glass transition at 54°C - highly disordered crystallites [2]. Hence, growth rates are generally low [3]. Directly associated with the slow structure evolution is the large size of the developing crystallites. The thicknesses of the crystal lamellae, which have a high lateral extension, are always above 10nm and go up to about 25nm at the highest crystallization temperatures [4][5][6].

In fact, the large crystal size and the low growth rate is advantageous for studies. Details show up which cannot be grasped in other crystallizing systems. Small angle X-ray scattering (SAXS) experiments end at a resolution of 1-2nm - then microscopic electron density fluctuations begin to affect the scattering curve - and have (under lab conditions) a time resolution of the order of minutes. For SAXS studies of PLLA this is still sufficient. We present in this contribution time- and temperature dependent experiments which provide insight into ordering processes at the surfaces of the crystallites and follow the kinetics of recrystallization processes. Wide angle X-ray scattering (WAXS) patterns which were registered simultaneously with the SAXS curves were analyzed by a simple new technique which detects deviations from a purely two-phase crystalline-amorphous structural development. We find clear indications for the participation of an additionally involved third state of order. Additionally conducted DSC experiments allowed a time resolution of the melting process. The unusual length scale of the crystalline-amorphous structure of PLLA is also favorable for an imaging by atomic force microscopy (AFM), as will be shown by high temperature scans of the PLLA structure after recrystallizations.

2 Experimental section

2.1 Sample

We prepared PLLA following the standard route as described, for example, in ref.[4]. Tin(II) 2-ethylhexanoate initiator was dissolved in dichloromethane and then dispersed in molten L-lactide with a molar ratio of 1:10000. This mixture was kept under argon in a tightly capped glass vial for 4 hours at 180°C for polymerization. To purify the polymer it was dissolved in gently warm chloroform, precipitated in methanol, filtered, and then dried under vacuum for several days. The molecular weights measured by gel permeation chromatography using PS standards are M_w=37700 and M_n=19200. Samples for X-ray scattering experiments were prepared by a rapid cooling of the melt at 200°C. Since the thermal stability of PLLA is low - decomposition begins already at 230°C [7] - we kept the annealing time in the melt always short.

2.2 Small angle X-ray scattering

SAXS experiments were carried out with the aid of a Kratky-camera attached to a conventional CuK_α X-ray source, employing a temperature controlled sample holder. Using a position-sensitive detector (PSD), scattering curves were usually registered within a few minutes counting time. After a deconvolution of the slit-smeared data, scattering curves were obtained in absolute values, as differential cross sections per unit volume $\Sigma(q)$. With a knowledge of $\Sigma(q)$ the one-dimensional electron density correlation function $K(z)$ can be directly calculated by applying the Fourier relation [8]

$$K(z) = \frac{1}{r_e^2} \int_0^\infty \cos(2\pi s) 4\pi s^2 \Sigma(s) \mathrm{d}s \ . \tag{1}$$

Here, s denotes the scattering vector $s = 2\sin\theta_B/\lambda$ (θ_B: Bragg scattering angle); r_e is the classical electron radius.

A useful parameter in kinetical measurements is the Porod coefficient P. It generally describes for two-phase systems the asymptotic behavior of the scattering curve as

$$\lim_{q\to\infty} \Sigma(s) = r_e^2 \frac{P}{s^4} \ . \tag{2}$$

The Porod coefficient is directly related to the interface area per unit volume, O_{ac}, by

$$P = \frac{1}{8\pi^3} O_{\mathrm{ac}} (\rho_{\mathrm{e,c}} - \rho_{\mathrm{e,a}})^2 \tag{3}$$

where $\rho_{\mathrm{e,c}}$ and $\rho_{\mathrm{e,a}}$ denote the electron densities of the crystals and the fluid phase respectively. This relation is generally valid, for homogeneous as well as heterogeneous structures and therefore, for example, also if spherulites fill a sample only partially.

2.3 Wide angle X-ray scattering

Simultaneous with the SAXS curves WAXS patterns were registered. For this purpose the Kratky camera was complemented by a second camera with an own PSD . It measures the scattering in the angular range $2\theta_B = 18^\circ - 26^\circ$ (product of Co. Hecus & Braun, Graz, Austria).

Usually it is assumed that WAXS curves measured during an isothermal crystallization represent a superposition of the scattering functions $I^{\mathrm{c}}(s)$ of the crystals and $I^{\mathrm{a}}(s)$ of the melt with weights given by the crystallinity ϕ_{c}, i.e.:

$$I(s) = \phi_{\mathrm{c}} I^{\mathrm{c}}(s) + (1 - \phi_{\mathrm{c}}) I^{\mathrm{a}}(s) \ . \tag{4}$$

$I^{\mathrm{a}}(s)$ is a smooth function with a maximum at the position of the halo. $I^{\mathrm{c}}(s)$ is dominated by the Bragg reflections of the crystal, but has also non-negligible contributions of diffuse scattering between the reflections due to disorder and thermal motions. It is possible to check in simple manner, if a crystallization can really be described by a change in the volume fraction ϕ_{c} and $(1 - \phi_{\mathrm{c}})$ of crystals and melt-like regions only. One chooses two locations s_1, s_2, for example one at a reflection maximum and the other in a range of purely diffuse scattering. The intensities of s_1 and s_2 are according to Eq.4

$$\begin{aligned} I(s_1) &= \phi_{\mathrm{c}} I^{\mathrm{c}}(s_1) + (1 - \phi_{\mathrm{c}}) I^{\mathrm{a}}(s_1) \\ I(s_2) &= \phi_{\mathrm{c}} I^{\mathrm{c}}(s_2) + (1 - \phi_{\mathrm{c}}) I^{\mathrm{a}}(s_2) \ . \end{aligned} \tag{5}$$

Differentiation with regard to ϕ_{c} gives

$$\frac{\mathrm{d}I(s_1)}{\mathrm{d}\phi_{\mathrm{c}}} = I^{\mathrm{c}}(s_1) - I^{\mathrm{a}}(s_1) \tag{6}$$

$$\frac{\mathrm{d}I(s_2)}{\mathrm{d}\phi_\mathrm{c}} \;=\; I^\mathrm{c}(s_2) - I^\mathrm{a}(s_2) \;\; .$$

Asking about the relationship between changes in $I(s_1)$ and $I(s_2)$ one can plot $I(s_1)$ versus $I(s_2)$ including values from all curves registered during the crystallization. If Eq.6 is valid, i.e., crystal and melt are the only phases involved in the crystallization process, a linear relationship between $I(s_1)$ and $I(s_2)$ is expected, with a slope given by

$$\frac{\mathrm{d}I(s_2)}{\mathrm{d}I(s_1)} = \frac{I^\mathrm{c}(s_2) - I^\mathrm{a}(s_2)}{I^\mathrm{c}(s_1) - I^\mathrm{a}(s_1)} = \mathrm{const} \;\; . \tag{7}$$

Deviations are indicative for the participation of states of order which differ from both the crystal and the melt.

2.4 DSC and AFM

The X-ray scattering experiments were complemented by DSC runs and AFM imaging. We used a Perkin-Elmer DSC7. AFM pictures were obtained with a PicoPlus (Molecular Imaging Co) in the tapping mode. Height- and phase-contrast images were recorded, thus probing the viscoelastic properties of the surface of film samples placed on a glass substrate. Employing a hot stage, temperature dependent experiments could be carried out in-situ. Samples were prepared in the molten state between two glass slides by pressing and removing the upper slide. Thicknesses were in the range of 1-10μm.

3 Results and Discussion

3.1 Surface ordering during isothermal crystallization

Figures 1, 2 and 3 present the results of a time-dependent SAXS and WAXS experiment, carried out during an isothermal crystallization at 145°C. Figure 1 shows the variation of the WAXS pattern in the lower part of the angular range covered by the detector. In the ranges around the two strongest Bragg-reflections (hkl=203 and 015) the intensity increases with time, outside these limited ranges one

observes a decrease. We compared the changes at the two indicated positions: s_1 in the center of the 203-reflection and s_2 which is outside of all reflections. The intensity at s_1, $I(s_1)$, is dominated by the crystals, the intensity $I(s_2)$ is mostly determined by the amorphous parts in the sample. Figure 2 shows this comparison in a plot of $I(s_1)$ versus $I(s_2)$. For some of the points the respective times are given. From the beginning up to 13500s one finds a linear relationship, as it is expected when crystals grow out of a melt. Interestingly, this linearity ends in the final time period between 13500 and 61500s. Here, points deviate from the initial line. Obviously the ordering process then changes its character.

The nature of the change becomes apparent in the electron density correlation functions $K(z)$ deduced from SAXS curves registered during the crystallization. Some of them are shown in Fig. 3, and they mostly refer to the time period between 13500 and 58500s. Within this late time range both the long spacing L and the inner surface $O_{\rm ac}$, being given by the initial slope of $K(z)$, remain constant. One observes, however, changes in the shape of the curves in the base region between 5nm and 15nm. According to the constant values of L and $O_{\rm ac}$ the stack formation is completed, but ordering processes still proceed in the intermediate range between the layer-like crystallites and the melt-like intercrystalline layers. The correlation function measured at the end of the crystallization process indicates the presence of crystals with a thickness $d_{\rm c} = 14$nm, layers with melt-like structure with a thickness $d_{\rm a} = 5$nm and an intermediate zone on both sides of the crystals with a total thickness of 2nm. The long spacing amounts to L=21nm. At an earlier time, 13500s, the intermediate region is much expanded, amounting to 5nm altogether, i.e., 2.5nm on each side. Figure 4 presents this change in a schematic drawing. The short linear section from z=7.5nm to 10nm in $K(z)$ given by the broken line in Fig. 3 relates to an intermediate layer. Its slope indicates, when compared to the initial slope of $K(z)$, a density change between the crystals and the intermediate layer in the order of 25% of the density difference between crystals and the melt. This ratio is included in the sketch. It means that the intermediate layer is much more crystal- than melt-like. With increasing time the inner part with crystalline order further expands into the region of the intermediate layer, and this surface ordering is indicated in Fig. 4. It implies a decrease in the free

energy, i.e., a stabilization of the crystallites.

In our view polymer crystallites do not form directly out of the melt, but use a pathway which includes a transient mesomorphic phase [9]. Based on this view one may identify the non-crystalline intermediate layer with remainings of the mesomorphic phase. Crystal growth would then proceed as is indicated in the sketch in Fig. 5. A region with a mesomorphic structure forms between the lateral crystal face and the melt, stabilized by epitaxial forces. A high inner mobility allows a spontaneous thickening up to a critical value where the core region crystallizes, which takes place under formation of a block. In the last step, the surface region of this block which remains at first in the mesomorphic phase, takes on the crystalline order. It is this last step which shows up in the experiment.

There were similar observations for an isothermal crystallization at $155^{\circ}\mathrm{C}$, as is shown by the SWAXS results presented in Figs. 6, 7, 8 and 9. Figure 6 depicts the time dependence of the Porod coefficient P and of the intensity $I(s_1)$ at the 203-Bragg reflection. According to the dependence $P(t)$ stack formation is finished at 80×10^3s. In contrast to that the crystallinity still increases, up to the end of the experiment by additional 15%.

Figure 7 displays three correlation functions derived from the SAXS curves during this late stage. Their change has the same character as the change of the correlation functions in Fig. 3. Shapes are again indicative for a transition zone between crystallites and melt-like layers, which is at first rather extended and then decreases in thickness. The thickness of the melt-like layer is comparable to that found in the first measurement. The long spacing has increased to 24nm at this higher crystallization temperature. The correlation function measured at 113×10^3s indicates a total thickness of the non-crystalline intermediate layer of $2\times$4nm. Within the time period of the experiment it becomes reduced to $2\times$2.5nm. The ordering process might still go on, but needs here a very long time to come to an end.

Figure 8 presents the development of the WAXS curves, and Fig. 9 analyses the changes in a plot of $I(s_1)$ versus $I(s_2)$. The relationship shows no longer an extended linear range. Hence, the transformation cannot be described just by a formation of crystallites out of the melt; the participation of an additional

state of order is obvious. The slope of the dotted line agrees with that of the line in Fig. 2. The final structure can therefore be described as being composed of melt and crystallites only. In time ranges with a steeper slope of the $I(s_1)/I(s_2)$ curve the melt is partly transferred into a mesomorphic rather than a crystalline state. On the other hand, in ranges with a less steep slope crystals form not only from the melt, but also out of a mesomorphic, i.e., amorphous but not melt-like phase.

3.2 Recrystallization during heating

Figure 10 presents the result of a temperature dependent SAXS experiment. A sample was isothermally crystallized at 145°C and then heated in stepwise manner, at first with steps of 5°C, then 3°C and finally 2°C. The figure shows the electron density correlation functions $K(z)$ derived from the scattering curves. The correlation function at the beginning is identical with that obtained at the end of the isothermal crystallization at 145°C given in Fig. 3. No changes occur up to 160°C, i.e., the initial structure remains stable over 15K. Then recrystallization processes set in. Each one of the subsequent temperature steps leads to an increase of the crystal thickness and the long spacing. This continues up to 176°C where the final melting begins. It is completed at 180°C. The curves include a characteristic feature. In the initial state $K(z)$ is horizontal in the base region between z=5nm and 14nm as it is expected for a stack of lamellar crystallites [8]. This property changes with the onset of recrystallization processes. From thereon the line in this range gets more and more inclined. Such a modification of the curve shape is indicative for the existence of the voids in the stack. A removal of single crystals from the stack in statistical manner leads in the scattering curve, and therefore also in the correlation function, to a superposition of a single crystallite scattering- or correlation-function. The correlation function of a single crystal is a triangle with a base length corresponding to the crystal thickness. The observed inclination is a consequence of this additional contribution.

In fact, AFM images of the structure produced by the recrystallization process show voids within the stack, and Fig. 11 presents an example. The picture on the left - both images were obtained with the

aid of the tapping technique - shows the structure resulting from an isothermal crystallization at 140°C. One observes regularly packed lamellae with a constant thickness and a large lateral extension. The image picked up a domain with edge-on orientation. The periodicity agrees with the long spacing in the SAXS scattering patterns. The image on the right shows the structure after heating to a temperature in the recrystallization range. One observes again a stack of lamellae but it now includes many voids. The periodicity in the image is larger than the long spacing, because the orientation of the stack here is not edge-on but inclined. Obviously recrystallization leads to a complete reorganization of the stack as a whole. The result of the reorganization is a new stack which has again well defined structural properties, i.e., certain values of the crystal thickness and the long spacing. As it appears, individual crystals do not retain their identity. Recrystallization is a cooperative phenomenon which concerns the whole stack at once.

In spite of the complexity of the process, recrystallization after temperature steps of some degrees is completed within short time. It obviously takes place quite rapidly. There exist, however, situations where the establishment of the new equilibrium after a temperature jump is slow so that it can be observed in real time. This is the case if a sample is directly transferred from the crystallization temperature into the temperature range of final melting, and Figs. 12 and 13 provide an example. A sample initially crystallized at 138°C was transferred as quickly as possible to a temperature of 174°C. Figure 12 depicts a series of SAXS curves measured one by one at this temperature. There is first a shift in the position of the long spacing reflection which is then followed by an intensity increase. The second maximum in the scattering curve whose position is determined by both, intracrystalline and intercrystalline properties, shows a continuous shift. The structural background of all the changes shows up in the electron density correlation function, and the deduced curves $K(z)$ are given in Fig. 13. The location of the minimum gives the crystal thickness, d_c, the following maximum relates to the long spacing L. One observes a change from d_c=13nm to 19nm and from L=21nm to L=30nm. Important to note, stability is reached within about $2 \cdot 10^3$s. One therefore observes here the kinetics of the establishment of a new stable

structure taking place under isothermal conditions. The structural changes observed within this time are only possible if the crystallites in the structure are not yet fixed, i.e., possess sufficient inner mobility. One might speculate that during this time period the core region of the crystallites has not yet reached that thickness which blocks any reformation. Support for such a view is given by the changing shape of the correlation function between z=0 and the d_{c}-determined minimum. As long as the structure is unstable this part of the curve shows a continuous bending. This apparently changes at later times. In the then measured curves existence of a melt-like layer of a thickness d_{a} $\approx$5nm is showing up more and more clearly. Hence, in the non-stable state the profile of the transition zone between crystal and the melt-like regions is diffuse, which changes when the structure solidifies.

3.3 Kinetics of melting

Melting processes are always rapid compared to the times required for the crystallization, so that it is usually impossible to follow in experiments the melting process in real time. PLLA presents an exceptional case. Crystallites grown at higher temperatures are unusually thick with values up to 25nm. For such crystals the separation of chain sequences from their lateral faces requires an unusually long time. It is still not long enough to enable the melting process to be followed in real-time scattering experiments under lab conditions, however, in the DSC clear time dependent effects show up during melting. One observes a pronounced superheating and Fig. 14 gives an example. It includes two melting curves, measured after an isothermal crystallization at 140°C. As can be seen, an increase of the heating rate from 1K/min to 10K/min results in an upward temperature shift of 5K. The superheating effect indicates that the melting needs a measurable time. Figure 15 provides a second example. The sample, isothermally crystallized at 140°C was heated into the melting range to 170°C. Experiments show the time dependence of melting at 170°C. Keeping the sample at 170°C leads within the first 5 minutes to a reduction of the amplitude of the high temperature endotherm associated with the melting of the remaining crystallites. For longer times of storage melting is followed by a new crystallization, as shown by the again

increasing peak amplitude. Rather than directly continuing the heating after the storage at 170°C samples were first rapidly cooled back to 140°C. The low temperature endotherm in the shown thermograms relates to the melting of crystallites formed during the cooling. Comparing the curves for 0min, 1min and 5min time of residence at 170°C, this first peak increases in amplitude while the second peak decreases.

Acknowledgements

Support of this work by the Deutsche Forschungsgemeinschaft is gratefully acknowledged. Thanks are also due to the Fonds der Chemischen Industrie for financial help.

References

[1] J. De Santis, P. Kovacs. *Biopolymers*, 6:299, 1968.

[2] J. Zhang, Y. Duan, H. Sato, H. Tsuji, I. Noda, S. Yan, and Y. Ozaki. *Macromolecules*, 38:8012, 2005.

[3] M.L. Di Lorenzo. *Eur.Polym.J.*, 41:569, 2005.

[4] J. Huang, M.S. Lisowski, J. Runt, E.S. Hall, R.T. Kean, N. Buehler, and J.S. Lin. *Macromolecules*, 31:2593, 1998.

[5] S. Baratian, E.S. Hall, J.S. Lin, R. Xu, and J. Runt. *Macromolecules*, 34:4857, 2001.

[6] T.Y. Cho and G. Strobl. *Polymer*, 47:1036, 2006.

[7] S.H. Lee, B.S. Kim, S.H. Kim, S.W. Kang, and Y.H. Kim. *Macromol.Biosci.*, 4:802, 2004.

[8] G. Strobl. *The Physics of Polymers*, page 498. Springer, 1997.

[9] G. Strobl. *Eur.Phys.J.E*, 18:295, 2005.

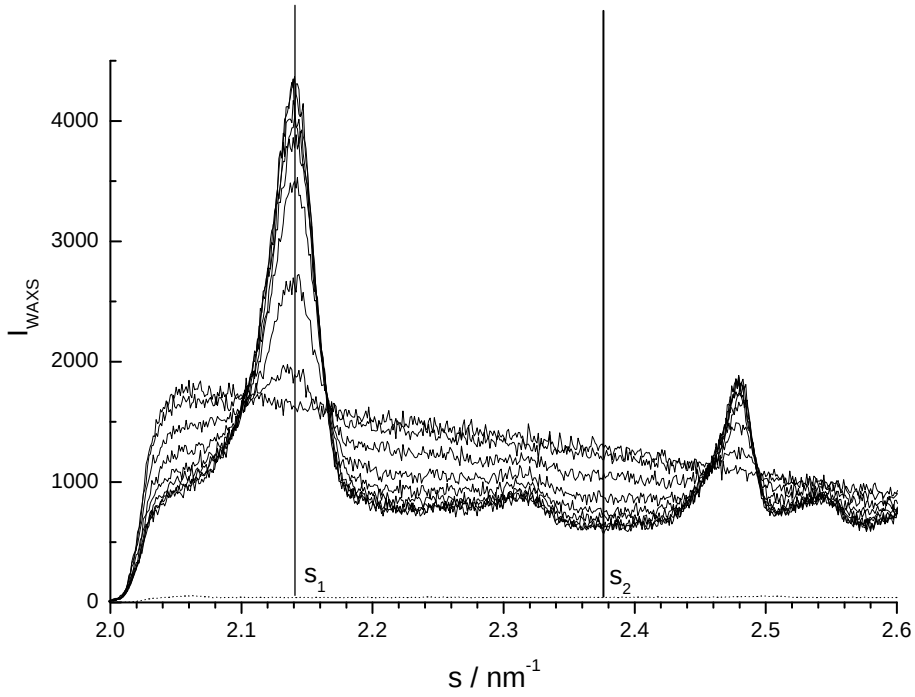

Figure 1: PLLA, crystallization at 145°C: Change of the WAXS curves with time. Positions selected for a crystal-dominated scattering (s_1) and a melt-dominated scattering (s_2)

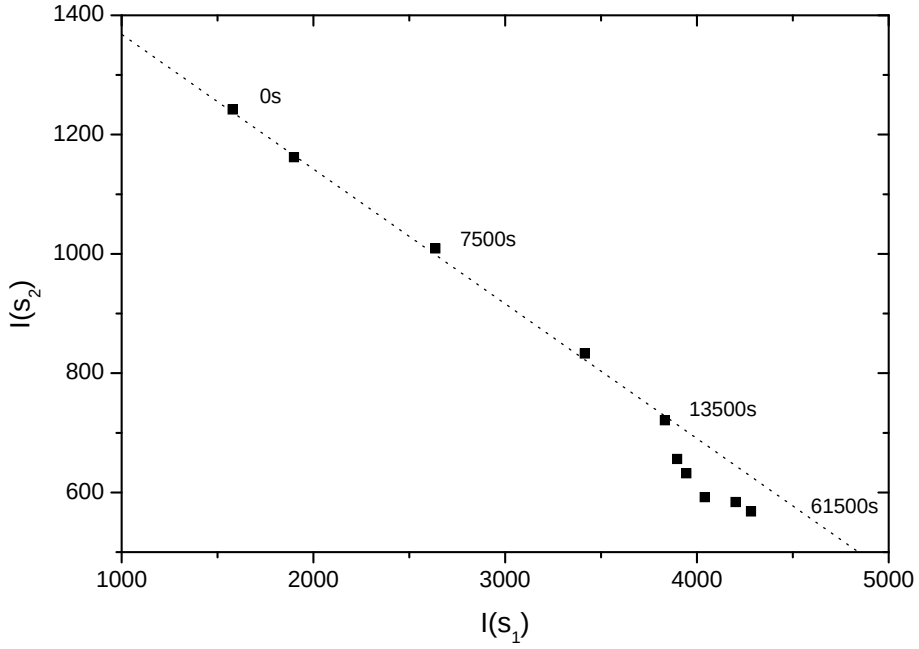

Figure 2: PLLA, crystallization at 145°C: Correlation between the changing WAXS intensities $I(s_1)$ and $I(s_2)$

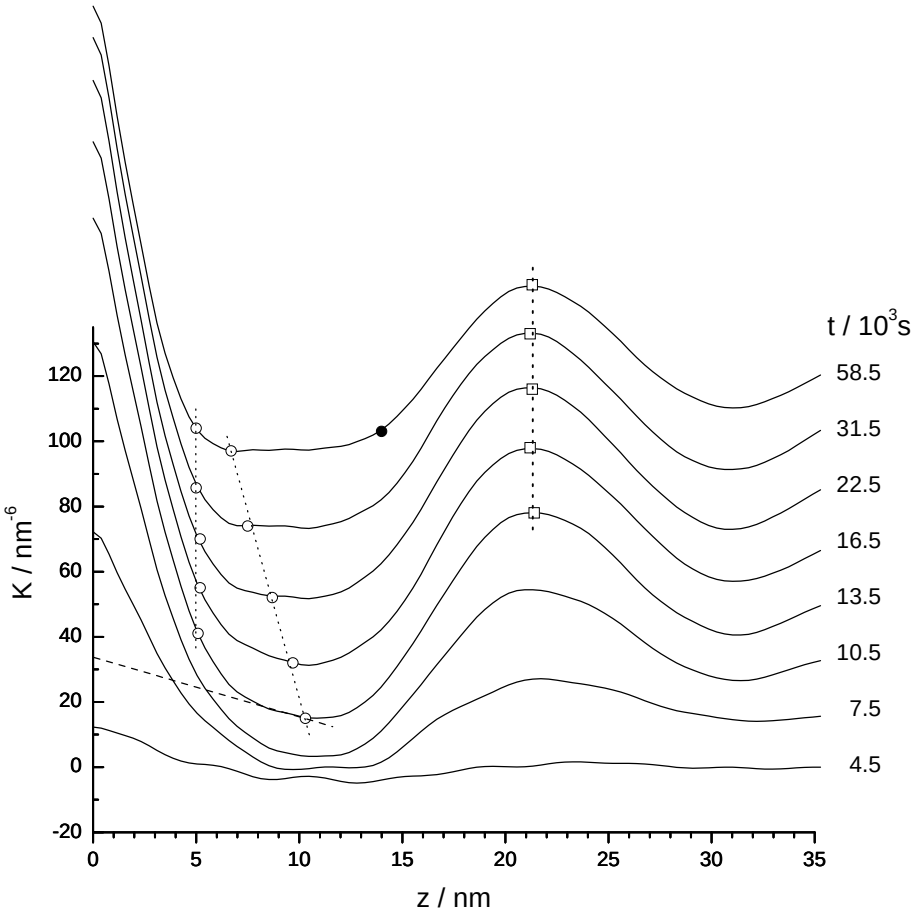

Figure 3: PLLA, crystallization at 145°C: Electron density correlation functions $K(z)$ determined by SAXS measurements at the given times. The locations of the symbols give - with increasing z - the thickness d_{a} of melt-like layers, the total thickness of the non-crystalline region, the crystal thickness d_{c} (*filled circle*), and the long spacing L (*squares*)

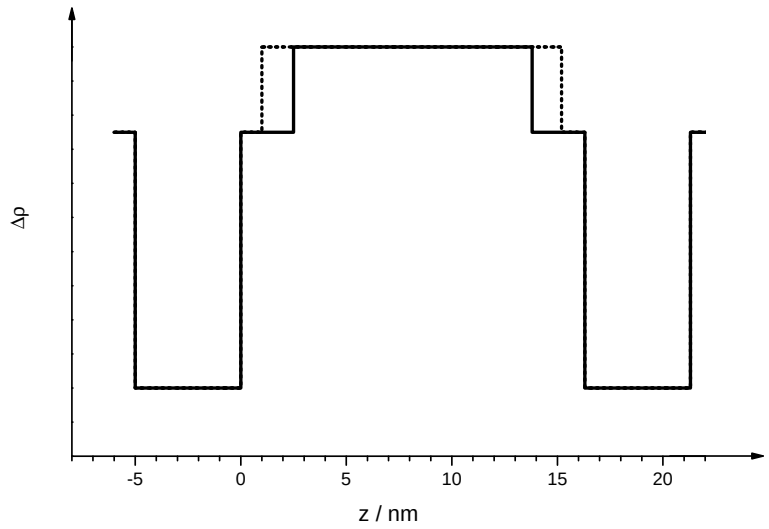

Figure 4: Electron density profile along the stack normal indicated by the correlation function at $t = 13.5 \times 10^3$ and $t = 58.5 \times 10^3$ (*dashes*) respectively

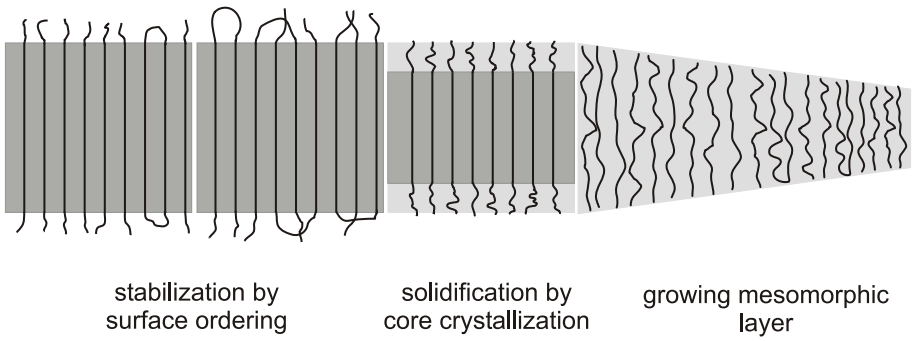

Figure 5: Sketch of a possible pathway followed in the growth of polymer crystallites

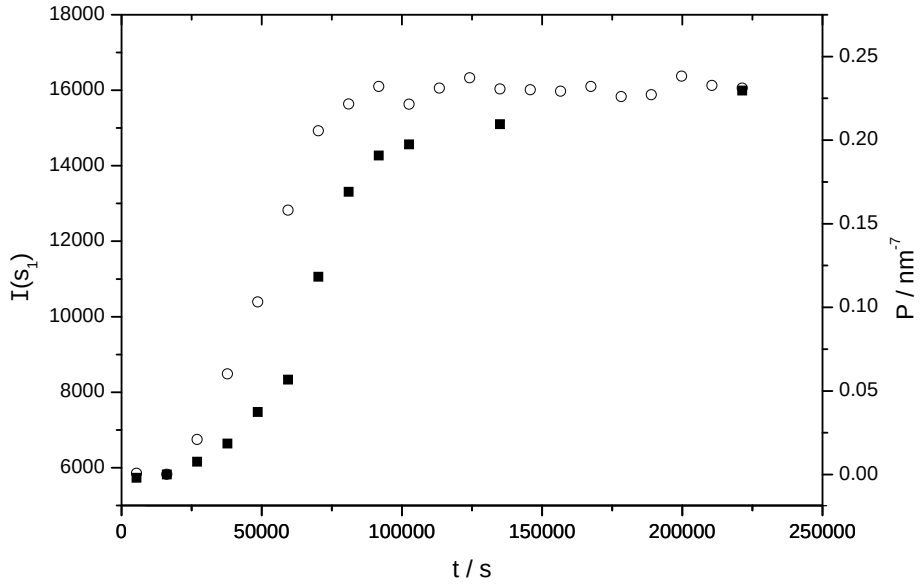

Figure 6: PLLA, crystallization at 155°C: Changes with time of the Porod coefficient P (*circles*) and of the WAXS intensity $I(s_1)$ (*squares*)

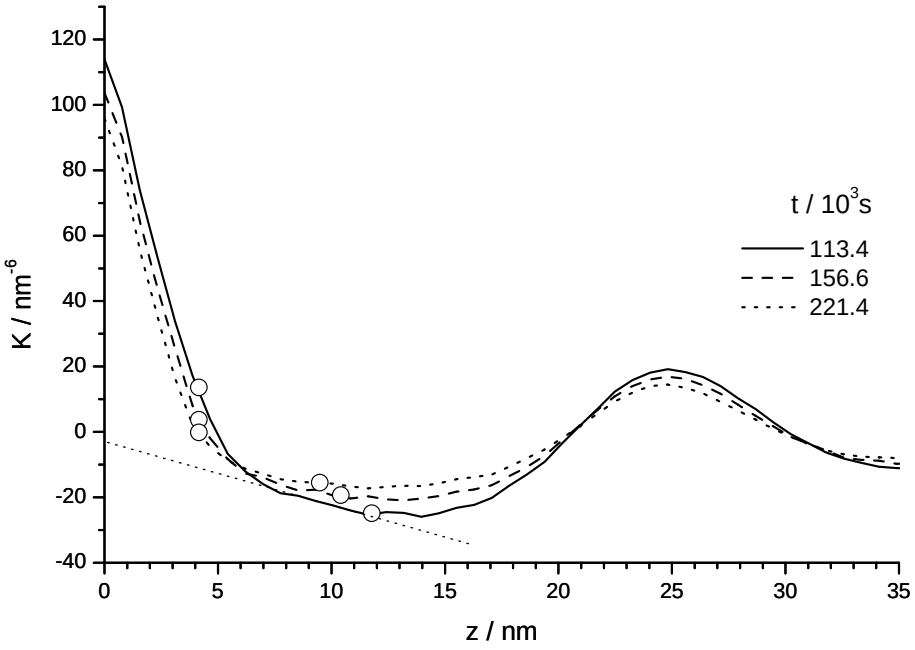

Figure 7: PLLA, crystallization at 155°C: Electron density correlation functions $K(z)$ derived from SAXS measurements in the late time period. Circles give the thickness of the melt-like layers and the total thickness of non-crystalline regions

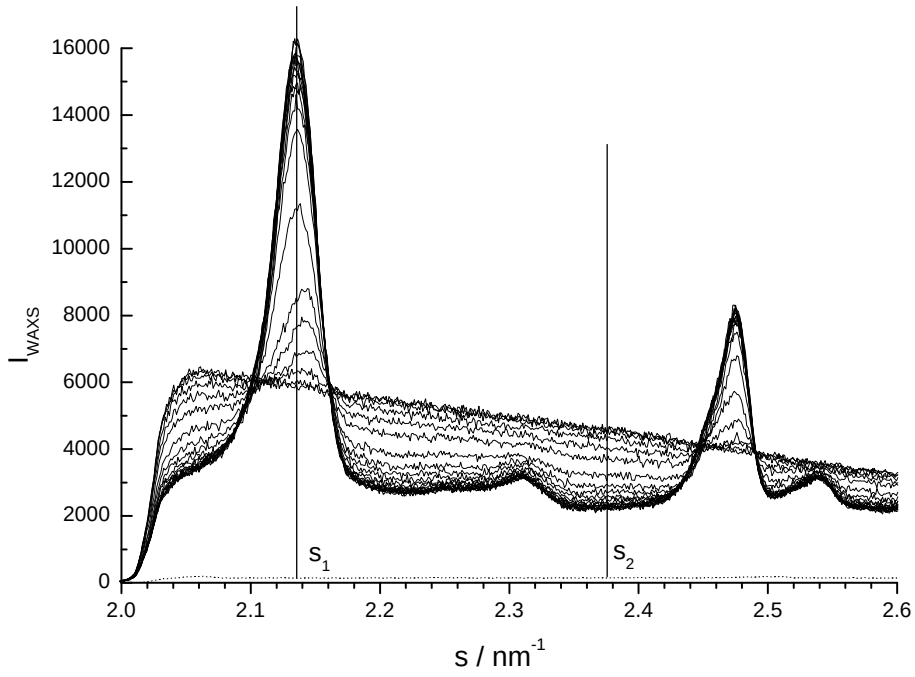

Figure 8: PLLA, crystallization at 155°C: Change of the WAXS curves with time

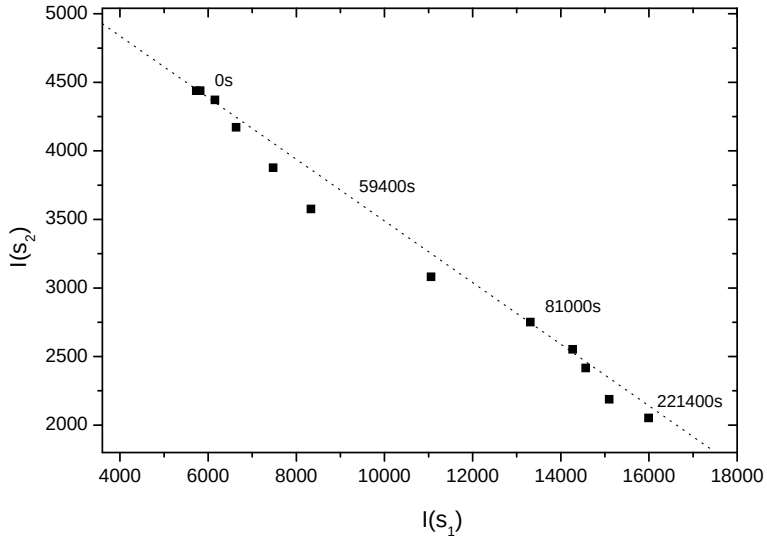

Figure 9: PLLA, crystallization at 155°C: Correlation between the changing WAXS intensities $I(s_1)$ and $I(s_2)$

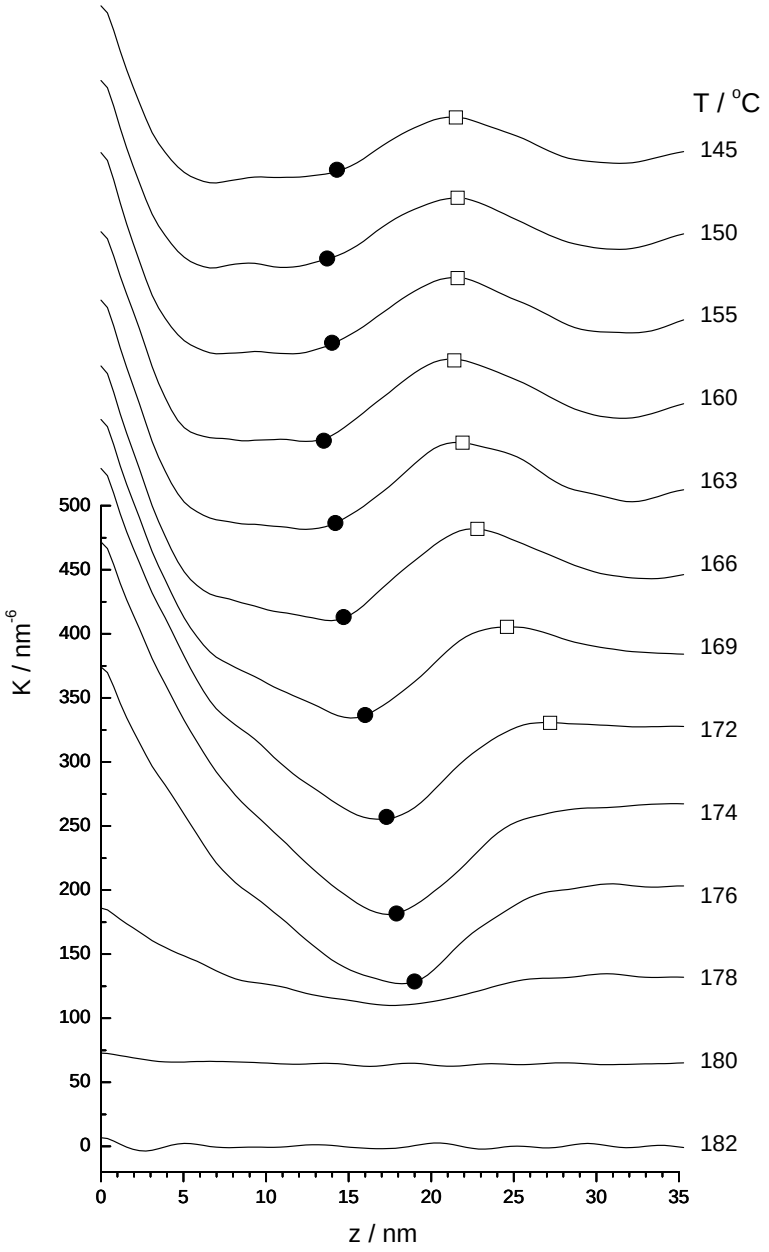

Figure 10: PLLA, step-wise heating after a crystallization at 145°C: Electron density correlation functions derived from SAXS curves measured at the given temperatures. The locations of the two symbols on the curves give the crystal thickness (*circles*) and the long spacing (*squares*)

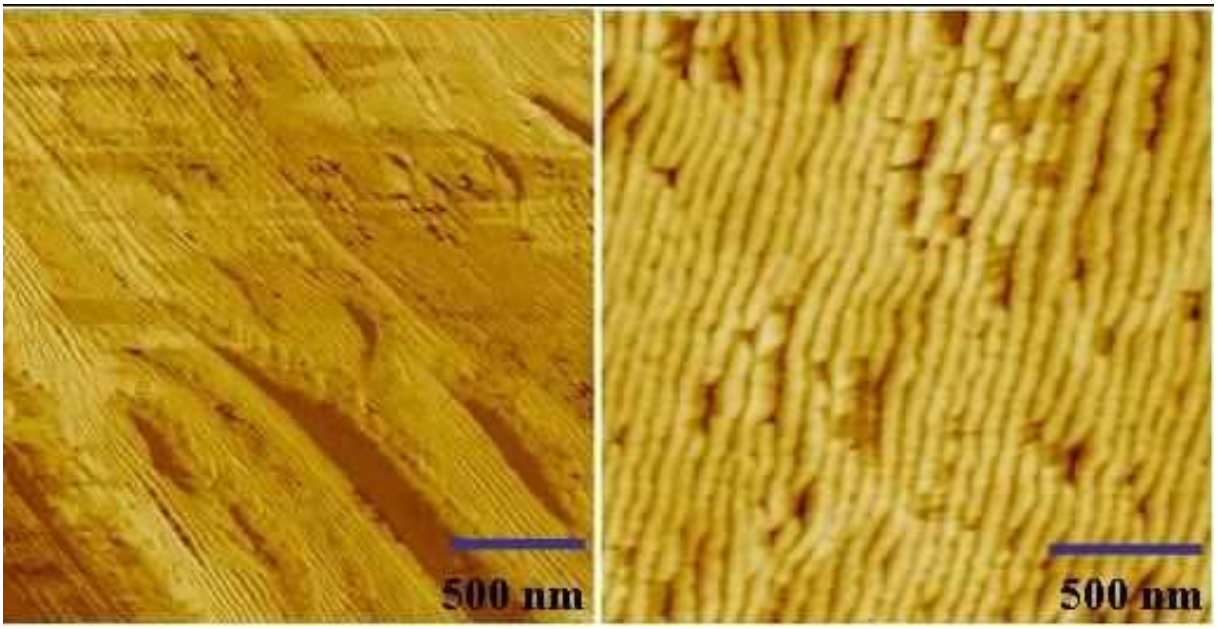

Figure 11: PLLA, crystallized at 140°C (*left*) and heated to 170°C (*right*): AFM tapping mode phase contrast images obtained after cooling to room temperature

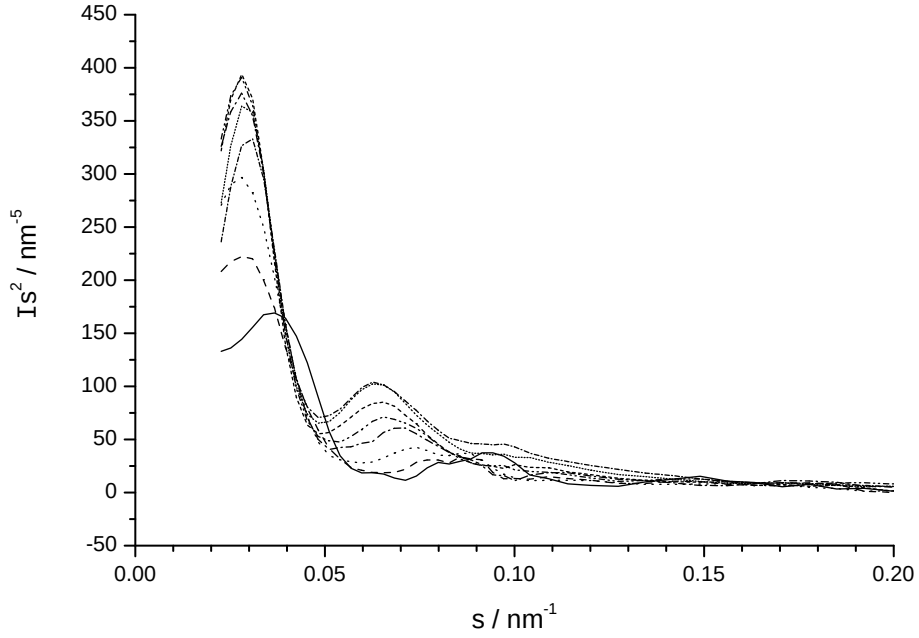

Figure 12: PLLA, crystallized at 138°C and rapidly transferred to 174°C: SAXS curves measured during the structure reformation

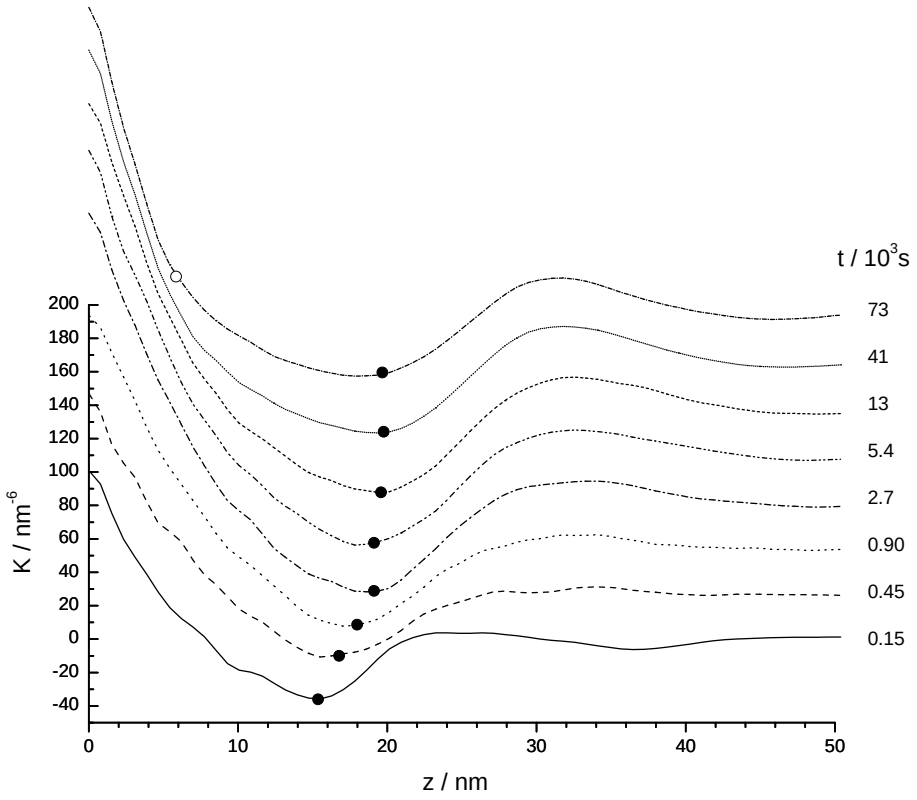

Figure 13: PLLA, recrystallization at 174°C: Correlation functions deduced from the SAXS curves in Fig.12. The locations of the filled circular symbols at the minima give d_{c}, the open symbol in the uppermost curve relates to d_{a}

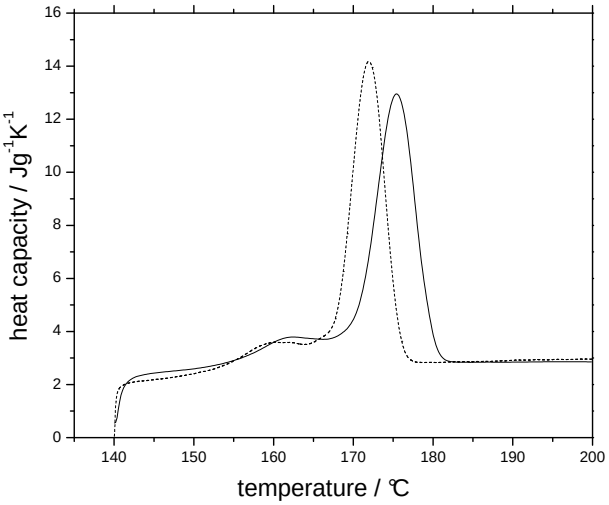

Figure 14: PLLA crystallized at 140°C: DSC thermograms recorded with heating rates of 10K/min and 1K/min (*dotted*)

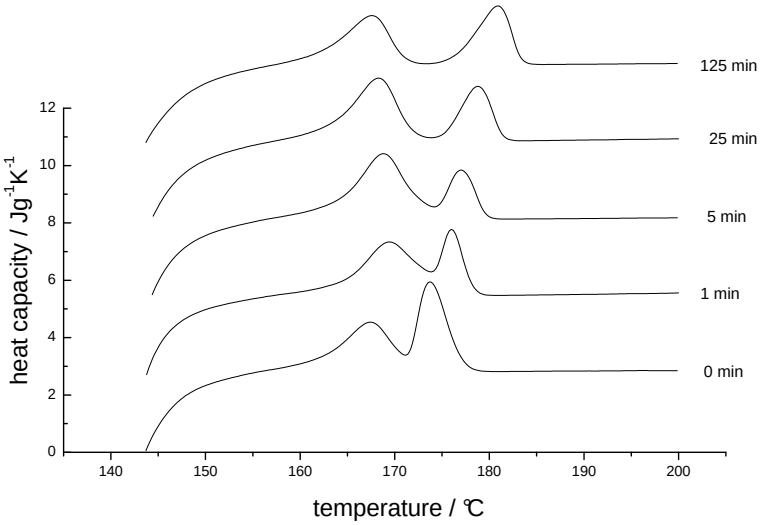

Figure 15: PLLA, crystallized at 140°C, heated to 170°C, annealed for 0 - 125 min, rapidly cooled to 140°C: Thermograms obtained during a heating to the melt. The variations are indicative for a time-dependent melting-recrystallization process at 170°C